Chlamydomonas reinhardtii formin and profilin are optimized for acute rapid actin filament assembly

Jenna R. Christensen[a], Michael J. Glista[a], David M. Mueller[b], Yujie Li[a], Jennifer A. Sees[a], Colleen T. Skau[a], Laurens J. Mets[a], Prachee Avasthi[b,c*], and David R. Kovar[a,d*]

[a]Department of Molecular Genetics and Cell Biology
The University of Chicago, Chicago, IL 60637, USA
[b]Department of Anatomy and Cell Biology
University of Kansas Medical Center, Kansas City, KS 66103
[c]Department of Ophthalmology
University of Kansas Medical Center, Kansas City, KS 66103
[d]Department of Biochemistry and Molecular Biology
The University of Chicago, Chicago, IL 60637, USA

*Co-corresponding authors

Address correspondence to:

Prachee Avasthi
3901 Rainbow Boulevard
MS 3051, 2089 HLSIC
Kansas City KS 66103

E-mail: pavasthi@kumc.edu
Phone: 913-588-7344

David R. Kovar
The University of Chicago
920 East 58th Street
CLSC 214
Chicago, IL 60637

E-mail: drkovar@uchicago.edu
Phone: 773-834-2810

Running head: *Chlamydomonas reinhardtii* formin CrFor1
Key words: *Chlamydomonas reinhardtii,* actin, formin, profilin

Abbreviations: PRM, proline rich motif; TIRF, total internal reflection fluorescence

ABSTRACT

Chlamydomonas reinhardtii is a unicellular green alga that appears less dependent upon its actin cytoskeleton than other cell types for fundamental processes like division and polarization. Null mutants of actin in *Chlamydomonas*, as well as treatment with actin depolymerizing drugs, have only mild defects. The reduced dependence on the actin cytoskeleton is now known to be due to the expression of a non-conventional actin in these cells which has both overlapping and unique functions. One structure that contains almost exclusively conventional F-actin is the mating fertilization tubule of gametes as actin depolymerizing drugs and conventional actin mutants have impaired fertilization tubule formation. Therefore, *Chlamydomonas* provides an excellent system to investigate regulation of the actin cytoskeleton, and in particular, how actin polymerization occurs at a very specific place and time. Interestingly, while it may contain a functionally minimal actin cytoskeleton, *Chlamydomonas* expresses both a profilin (CrPRF) and a formin (CrFor1). We have found that unlike typical profilins, CrPRF inhibits both F-actin nucleation and barbed end elongation at equimolar concentrations to actin. However, CrFor1 overcomes the low polymerizability of CrPRF-bound actin and stimulates rapid actin filament assembly. CrPRF further favors CrFor1-mediated actin assembly by potently inhibiting Arp2/3 complex-mediated actin assembly. Together, these findings suggest that CrFor1 and CrPRF work together to selectively and rapidly assemble F-actin at the right time and place. In vivo results demonstrate that this rapid actin assembly by CrFor1 is important specifically for fertilization tubule formation during mating, as formin inhibitor SMIFH2 inhibits formation of fertilization tubules in *Chlamydomonas* gametes.

INTRODUCTION

The actin cytoskeleton is a dynamic system important for diverse cellular processes. *Chlamydomonas reinhardtii* expresses a single conventional actin, IDA5, with 90% identity to mammalian actin, as well as an unconventional actin, NAP1 (Lee *et al.*, 1997; Kato-Minoura, 1998) with low identity to mammalian actin (64%). Despite two actin genes, few F-actin networks have been identified in *Chlamydomonas*. An anti-actin antibody identified actin surrounding the nucleus during interphase (Harper *et al.*, 1992). This actin relocalizes throughout the cell cycle, moving from the anterior of the cell during preprophase and metaphase to the cleavage furrow during cytokinesis (Harper *et al.*, 1992). The antibody-labeled actin networks are also not stained by the fluorescent phallotoxin phallicidin (Harper *et al.*, 1992), suggesting that they may be composed of actin monomers or short actin filaments. Furthermore, actin depolymerizing Latrunculin B (LatB) drug treatment does not inhibit cell division (Kato-Minoura *et al.*, 1997). While this may appear to confirm that cleavage furrow localized actin is monomeric, this function may performed by LatB-insensitive NAP1 (Onishi *et al.* 2016). which is upregulated during LatB treatment. Direct F-actin labeling using the fluorescent Lifeact peptide also showed perinuclear localization during interphase (Avasthi *et al.*, 2014) .This perinuclear pool of F-actin is lost upon LatB treatment but is replaced by what are likely Lifeact-binding NAP1 filaments within 1 hour (Onishi *et al.* 2016). F-actin also localizes at the base of the flagella, where it is important for intraflagellar transport

(Avasthi *et al.*, 2014), However, the nature of this F-actin network awaits further characterization.

One clearly defined conventional F-actin network in *Chlamydomonas* is the fertilization tubule. The fertilization tubule is an F-actin-rich structure found in mating type plus gametes (Detmers *et al.*, 1983; 1985), which during mating protrudes from the 'doublet zone', a region between the two flagella (Detmers *et al.*, 1983). Phallicidin staining of F-actin strongly labels fertilization tubules (Detmers *et al.*, 1985), null mutants lacking conventional actin cannot form fertilization tubules (Kato-Minoura, 1998), and isolation of fertilization tubules revealed that actin is a major component (Wilson *et al.*, 1997). The context-dependent formation of this well-defined F-actin structure in *Chlamydomonas* provides an exceptional opportunity to understand how a cell is capable of precisely regulating its actin cytoskeleton so that actin polymerization occurs only at a very specific place and time.

Chlamydomonas expresses a profilin (CrPRF) which inhibits both the nucleation and nucleotide exchange of actin monomers, suggesting that CrPRF prevents unwanted actin assembly (Kovar *et al.*, 2001b). We have identified a *Chlamydomonas* formin (CrFor1) actin assembly factor, which has not been characterized and its cellular role in *Chlamydomonas* not yet determined. Therefore, we sought to characterize the formin CrFor1 and determine how CrFor1 assembles actin monomers bound to CrPRF. Additionally, we wished to determine the role of CrFor1 in *Chlamydomonas* cells. We found that CrPRF prevents actin assembly on its own by inhibiting both nucleation and elongation of actin filaments at relatively low concentrations. CrFor1 is capable of overcoming this inhibition and rapidly assembling CrPRF-bound actin monomers. Additionally, we found that *Chlamydomonas* cells treated with the formin inhibitor SMIFH2 do not form fertilization tubules, suggesting that the collective activities of CrPRF and CrFor1 regulate acute F-actin assembly specifically for mating in *Chlamydomonas*.

RESULTS

CrPRF inhibits nucleation and elongation of actin filaments

In cells, the majority of unassembled G-actin is bound to profilin (Carlsson *et al.*, 1977; Kaiser *et al.*, 1999; Lu and Pollard, 2001). Profilin inhibits the nucleation of new actin filaments, but once an actin filament has been formed, profilin-bound actin monomers readily add to the barbed end of growing actin filaments (Pollard and Cooper, 1984) Additionally, mammalian profilins promote ADP-to-ATP exchange within their bound actin, though plant profilins do not (Mockrin and Korn, 1980; Goldschmidt-Clermont *et al.*, 1991; Perelroizen *et al.*, 1994; 1996)

Chlamydomonas profilin CrPRF is found throughout the cytoplasm and flagellar compartments of the cell, but is enriched at the base of the flagella in vegetative cells and below the fertilization tubule in mating type + gametes (Kovar *et al.*, 2001). Previous work showed that unlike typical profilins, CrPRF inhibits the nucleotide exchange of bound G-actin, suggesting that CrPRF might inhibit actin assembly in cells more potently than other profilins potentially explaining the lack of abundant F-actin networks in *Chlamydomonas*. Consistent with its role as a potent actin polymerization inhibitor, we confirmed that actin assembly was inhibited in the presence of CrPRF in a

concentration-dependent manner (Figure 1A). Surprisingly, by directly observing the spontaneous assembly of 1.5 μM Mg-ATP actin monomers using Total Internal Reflection Fluorescence (TIRF) microscopy, we found that CrPRF inhibits not only nucleation, but also significantly inhibits elongation of actin filaments at concentrations where the ratio of CrPRF to actin is equal (Figure 1B), suggesting that CrPRF is a potent inhibitor of actin polymerization.

As actin filament formation in *Chlamydomonas* is restricted to specific cellular subdomains, an inhibitory profilin such as CrPRF could be ideal for proper F-actin organization by preventing spontaneous actin assembly. However, F-actin polymerization within the fertilization tubule still needs to occur at the correct time and place during mating. Therefore, we speculated that an actin assembly factor such as a formin may be responsible for rapid actin assembly at fertilization tubule sites.

Identification of a formin in *Chlamydomonas reinhardtii*

A BLAST search for conserved formin homology 2 (FH2) domain lasso and post sequences identified gene locus Cre05.g232900 in the *Chlamydomonas* genome. This gene encodes a transcript that contains an FH2 domain as well as a formin homology 1 (FH1) domain with three identifiable proline rich motifs (PRMs). However, a single base frameshift in the predicted sequence yields a transcript containing 7 additional PRMs for a total of 10 PRMs in the FH1 domain. Expressed Sequence Tag (EST) analysis confirmed that an expressed transcript contained 10 PRMs (Susan Dutcher, personal communication). We created bacterial expression constructs containing both 3 and 10 PRMs and confirmed their ability to stimulate actin polymerization (Figure 2), suggesting that the expressed protein is a formin. The formin was named *Chlamydomonas reinhardtii* formin 1 (CrFor1).

CrFor1 efficiently nucleates but weakly elongates actin filaments

Formins are a conserved family of actin assembly factors that both nucleate and processively elongate actin filaments (Breitsprecher and Goode, 2013). Formins contain actin assembly FH1 and FH2 domains, which are typically flanked by regulatory regions. Functional formins are dimers, with two FH2 domains interacting head-to-tail to create a donut-shaped dimer capable of creating a stable actin 'nucleus' (Otomo *et al.*, 2005). In addition, the FH2 dimer maintains processive association with the elongating barbed end of an actin filament (Kovar, 2006). The unstructured FH1 domains are rich in PRMs that bind to profilin and promote rapid association of profilin-actin with the barbed end of an elongating filament. In order to investigate the actin assembly properties of the formin CrFor1, we created a set of constructs containing the CrFor1 FH1 and FH2 domains, alone or in combination (Figure 2A).

CrFor1's capacity to stimulate actin assembly was initially investigated by measuring the effect of CrFor1 on actin polymerization over time using spontaneous pyrene actin assembly assays. CrFor1 containing the FH2 alone (CrFor1(FH2)) or both the FH1 and FH2 domains (CrFor1(3P,FH2) and (10P,FH2)) all stimulate actin assembly similarly and in a concentration-dependent manner (Figure 2B-C), and more efficiently than a well-characterized control formin fission yeast Cdc12(FH1,FH2) (Figure 2B-C) (Kovar *et al.*, 2003; Scott *et al.*, 2011). Though these results indicate that CrFor1 increases the overall rate of actin polymerization, spontaneous pyrene actin

assembly assays are unable to differentiate between an increase in the nucleation and/or elongation of actin filaments.

In order to differentiate between the contributions of nucleation and elongation to the overall enhanced polymerization rate, we first examined the effect of CrFor1 on actin filament elongation using seeded pyrene actin assembly assays. In the presence of actin filament seeds, the effect of actin polymerization due to nucleation of new filaments is minimized, and the elongation of existing seed barbed ends is the primary factor involved in the observed actin assembly rates. Adding CrFor1(FH2), CrFor1(3P,FH2) and CrFor1(10P,FH2) to seeded assembly reactions all reduced the rate of actin assembly in a concentration dependent matter (Figure 2D-E), suggesting that CrFor1 inhibits actin filament elongation, and that the increased actin assembly rate observed in spontaneous pyrene actin assays is due to CrFor1-mediated nucleation. Fits of the initial rate of polymerization over a range of formin concentrations, revealed dissociation rate constants (K_d) in the low nanomolar range. The affinities of the formin constructs for filament barbed ends were similar for CrFor1(FH2) (K_d=1.6 nM), CrFor1(3P,FH2) (K_d=0.17 nM), CrFor1(FH1,FH2) (K_d=0.24 nM), and Cdc12(FH1,FH2) (K_d=0.33 nM) (Figure 2E).

Similarly, CrFor1 also inhibits barbed end disassembly. In the presence of CrFor1 FH1 and FH2 fragments, the rate of F-actin depolymerization was significantly reduced over a range of concentrations (Figure 2F-G). Curve fits revealed affinities for the filament barbed ends similar to those determined by seeded assembly for CrFor1(FH2) (K_d=0.40 nM), CrFor1(3P,FH2) (K_d=0.40 nM), CrFor1(10P,FH2) (K_d=0.68 nM), and Cdc12(FH1,FH2) (K_d=0.76 nM) (Figure 2G). Together, these results indicate that CrFor1 potently stimulates actin nucleation, while inhibiting actin filament elongation. In addition, like other formins, CrFor1 binds actin filament barbed ends with an affinity in the low nanomolar range.

Fission yeast profilin SpPRF enhances CrFor1-mediated actin assembly

We have demonstrated that *Chlamydomonas* formin CrFor1 has potent nucleation activity but poorly elongates actin filaments. Similarly, in the absence of profilin, the fission yeast formin Cdc12 has high nucleation activity, but poorly elongates actin filaments. However, in the presence of fission yeast profilin SpPRF, Cdc12 rapidly elongates actin filaments (Kovar *et al.*, 2003; Scott *et al.*, 2011). We speculated that CrFor1 may similarly utilize profilin to rapidly elongate F-actin. We first tested the ability of profilin CrPRF to bind to the FH1 domains of CrFor1 and Cdc12. Interestingly, although CrPRF binds much more weakly than SpPRF to poly-L-proline (Figure 3A, C (Kovar *et al.*, 2001), CrPRF and SpPRF have similar affinities for the FH1 domains of both CrFor1 and Cdc12 (Figure 3B,C), all within the low micromolar range.

Although CrPrf1 binds well to the CrFor1 FH1 domain, the capacity of a formin to add profilin-actin to filament barbed ends depends on the complementarily of profilin with both the FH1 and FH2 domains of the formin (Neidt *et al.*, 2009; Bestul *et al.*, 2015). We initially tested the ability of CrFor1 to elongate SpPRF-bound actin, as SpPRF is widely compatible with different formin isoforms (Neidt *et al.*, 2009; Bestul *et al.*, 2015). Spontaneous pyrene actin assembly assays revealed that a CrFor1 construct containing both the FH1 and FH2 domains (CrFor1(3P,FH2)) rapidly accelerates actin assembly in the presence of fission yeast profilin SpPRF (Figure 3D-E). Conversely,

SpPRF inhibits actin assembly by CrFor1(FH2), the construct lacking the FH1 domain (Figure 3D-E). The pyrene actin assembly rates measured for CrFor1(3P,FH2) with SpPRF are greater than those of Cdc12(FH1,FH2) with SpPRF over a range of SpPRF concentrations (Figure 3E), indicating that SpPRF enhances the actin assembly of CrFor1(3P,FH2), presumably by dramatically increasing the processive elongation rate.

CrPRF-bound actin is utilized specifically by CrFor1

We next examined the ability of CrFor1 to assemble actin bound to CrPRF. In spontaneous pyrene actin assembly assays, the pyrene fluorescence measured in reactions containing CrFor1 and CrPRF is sharply reduced relative to actin alone or actin in the presence of CrFor1 (Figure 3F). While this could indicate that CrPRF severely inhibits CrFor1-mediated actin assembly, it is also possible that the combination of CrFor1 and CrPRF prevents assembly of actin labeled on Cys-374 with pyrene, as we have described for other formin and profilin combinations (Kovar *et al.*, 2006; Scott *et al.*, 2011). Therefore, we directly visualized actin filaments formed in spontaneous pyrene actin assembly assays in the presence of different combinations of formin and profilin. After assembling for 600 seconds, the bulk polymerization reactions were stopped by diluting into TRITC-Phalloidin to allow visualization of filaments by fluorescence microscopy (Figure 3G). In the absence of profilin, CrFor1 produces many small actin filaments (average length, 2.7 ± 4.0 μm), indicative of efficient nucleation by CrFor1. Conversely, CrFor1 facilitates formation of long actin filaments in the presence of both SpPRF (16.6 ± 10.2 μm) and CrPRF (27.4 ± 17.5 μm). Interestingly, although CrFor1 can utilize either SpPRF or CrPRF to elongate actin filaments, Cdc12 is unable to form long filaments in the presence of CrPRF (average length, 4.2 ± 4.9 μm) (Figure 3G), suggesting that CrPRF is tailored for elongation by CrFor1. Together, these results indicate that CrFor1 is capable of efficient actin filament nucleation, and in the presence of its complimentary profilin CrPRF, rapidly elongates these filaments. In addition, the inability of Cdc12 to elongate CrPRF-associated actin suggests that CrFor1 and CrPRF are tailored to precisely and rapidly polymerize F-actin.

CrFor1 rapidly and processively elongates actin filaments in the presence of CrPRF

To directly examine the effect of CrPRF on CrFor1-mediated actin assembly, we visualized the assembly of 1 μM Mg-ATP actin over time using TIRF microscopy. Actin filaments alone (control) elongate at a rate of 11.5 subunits per second (Figure 4A). In the presence of 1 nM CrFor1(3P,FH2), two populations of filaments were observed: actin filaments elongating at the control rate (9.1 sub/s, red arrowheads), and actin filaments elongating at a significantly slower rate (0.3 sub/s, blue arrowheads) (Figure 4B). Our interpretation is that the slow-growing filaments are bound at their barbed end by CrFor1, which inhibits their elongation, while filaments elongating at the control rate are not bound by CrFor1. In the presence of 1 nM CrFor1 and 2.5 μM CrPRF, two distinct populations of filaments are again observed: actin filaments elongating at a rate slower than the control rate (4.2 sub/s) and rapidly elongating actin filaments (63.2 sub/s) (Figure 4C). The assembly rate of internal control filaments is slower in these reactions because CrPRF inhibits actin filament elongation (Figure 1B), while CrFor1 can efficiently utilize CrPRF-bound actin to rapidly elongate actin filaments. The 200-

fold different in elongation rate for CrFor1 in the absence (~0.3 sub/s) and presence of CrPRF (~60 sub/s) is one of the largest observed (Kovar, 2006).

Our results suggest that CrFor1 and CrPRF work together to rapidly elongate F-actin. In order to directly visualize and confirm this finding, we created a SNAP-tagged construct of CrFor1(3P,FH2) capable of being labeled for multi-color TIRF microscopy experiments (Figure 5). In the absence of CrPRF, red-CrFor1 remains continuously associated with the barbed end of small, slow growing actin filaments (Figure 5A, blue arrowheads), consistent with our finding that CrFor1 can nucleate actin filaments but significantly slows actin filament elongation. Conversely, in the presence of CrPRF, CrFor1-associated actin filaments elongate rapidly (Figure 5B,D) compared to control filaments (Figure 5C).

CrPRF favors formin- over Arp2/3 complex-mediated assembly.

We found that CrPRF potently prevents spontaneous actin assembly by both inhibiting nucleation and barbed end elongation, whereas CrFor1 overcomes this inhibition and facilitates the assembly of rapidly elongating actin filaments. In addition to enhancing formin-mediated elongation, profilin has also been shown to tune F-actin network formation by inhibiting Arp2/3 complex-mediated actin filament branch formation (Rotty *et al.*, 2015; Suarez *et al.*, 2015). We speculated that CrPRF might be a particularly potent inhibitor of Arp2/3 complex by inhibiting both branch formation and subsequent elongation. We tested this possibility by performing bead assays in which fission yeast Arp2/3 complex activator Wsp1 or formin CrFor1 are attached to a polystyrene bead within a standard TIRF microscopy chamber (Figure 6). Actin alone and CrPRF-bound actin are subsequently flowed sequentially into the microscopy chamber to assess the effect of CrPRF on formin- and Arp2/3 complex-mediated actin assembly. When initially incubated with actin alone, CrFor1-bound beads poorly assembled F-actin (Figure 6D(1), E(1)), similar to what we observed in standard TIRF microscopy assays (Figure 4C, 5A). However, when CrPRF-bound actin was flowed into the TIRF chamber, rapid actin filament assembly occurred (Figure 6D(2), E(2)). Photobleaching the F-actin following the flow of CrPRF-bound actin showed a reoccurrence of high fluorescence at the bead (Figure 6D(3), F), indicative of rapid actin filament assembly by CrFor1 at the bead surface. Conversely, beads coated with Wsp1 showed normal actin assembly following incubation with actin and Arp2/3 complex (Figure 6A(1), E(1)). However, filament growth was halted following addition of CrPRF-bound actin (Figure 6B(2), E(2)). Photobleaching of F-actin shows very little new F-actin assembly at filament barbed ends, consistent with CrPRF inhibition of actin filament elongation. In addition, very little F-actin assembly occurs at the bead, demonstrating inhibition of Arp2/3 complex-mediated branch formation at the bead surface (Figure 6B(3), F).

Fertilization tubule formation is prevented by the formin inhibitor SMIFH2

CrPRF is a potent inhibitor of actin filament nucleation and elongation. However, CrPRF-bound actin can be rapidly assembled by CrFor1. As the fertilization tubule is known to be F-actin rich and appears by EM to contain a parallel array of linear actin filaments in *Chlamydomonas* (Detmers *et al.*, 1983), we suspected that CrFor1 might be required for fertilization tubule formation in *Chlamydomonas* gametes. To test this, we chemically induced fertilization tubule formation in gametes and stained cells with

fluorescent phalloidin to label F-actin (Figure 7B-H). 1% DMSO treated controls showed fertilization tubules in ~43% of cells (Figure 7B, C and H). As expected, treatment with 10 μM latrunculin B, which depolymerizes F-actin networks, completely eliminated fertilization tubules (Figure 7D, H).

Formin inhibitor SMIFH2 potently inhibited CrFor1-mediated actin assembly in vitro (Figure 7A, Rizvi *et al.*, 2009). Correspondingly, though 10 μM formin inhibitor SMIFH2 had little effect on tubule formation (Figure 7E, H), only ~5% of gametes formed fertilization tubules in the presence of 100 μM SMIFH2 (Figure 7F, H). To ensure that fertilization tubule loss with 100 μM SMIFH2 is specific, we also treated cells with 100 μM of Arp2/3 complex inhibitor CK-666 (Nolen *et al.*, 2009). CK-666 treated cells did not lose their fertilization tubules (Figure 7G, H), demonstrating that CrFor1-mediated but not Arp2/3-mediated F-actin assembly is required for fertilization tubule formation. Lastly, we found that CrFor1 is capable of bundling actin filaments to a similar extent as fission yeast formin Fus1, the formin involved in mating projectile formation in fission yeast cells (Figure S1), suggesting that CrFor1 could potentially be involved in bundling of actin filaments in the fertilization tubule.

Discussion

CrPRF as a regulator of F-actin assembly

We found that CrPRF is an unusual profilin that dramatically prevents unwanted actin assembly by inhibiting both the nucleation and elongation of actin filaments. Furthermore, CrFor1 is able to overcome the inhibitory effect of CrPRF and utilize CrPRF-bound actin to rapidly assemble actin filaments for the fertilization tubules in mating gametes. Conversely, CrPRF inhibits Arp2/3 complex-mediated actin assembly, providing a mechanism by which F-actin can be assembled at the precise time and place by CrPRF and CrFor1. We have previously shown that the profilin defines the rate of formin-mediated actin assembly (Neidt *et al.*, 2009). The presence of tailored formin-profilin pairs (Bestul *et al.*, 2015) suggests that this interaction is crucial for controlling utilization of an actin monomer pool. The *Chlamydomonas* profilin CrPRF appears to be an extreme example of this, as CrPRF-bound actin does not nucleate or elongate well in the absence of CrFor1. In more complex organisms, the presence of multiple profilin isoforms expressed at different levels could regulate network size by controlling actin utilization by different formin isoforms (Mouneimne *et al.*, 2012).

Inhibition of Arp2/3 complex-mediated branch formation and elongation could further bias *Chlamydomonas* towards CrFor1-mediated assembly, by preventing competition for actin monomers (Suarez *et al.*, 2015; Suarez and Kovar, 2016). *Chlamydomonas* expresses components of the Arp2/3 complex, but its activators have not been identified (Kollmar *et al.*, 2012). The Arp2/3 complex may be involved in assembly and maintenance of the F-actin involved in flagellar protein trafficking, as treatment with Arp2/3 complex inhibitor CK-666 induces flagellar shortening (Avasthi *et al.*, 2014). The presence of other potential F-actin networks provides the additional possibility that other F-actin assembly factors are also present in *Chlamydomonas*. The inability of latrunculin and cytochalasin treatments to affect cytokinesis may be a result of their inability to bind NAP1, which is upregulated upon conventional actin disruption and can likely compensate for disrupted conventional actin. Future work will involve

determining the nature of the F-actin networks involved in cytokinesis and flagellar protein trafficking and CrPRF's role in ensuring proper F-actin distribution to each network.

CrFor1 in fertilization tubule formation

CrFor1 is required for fertilization tubule formation as treatment with the formin inhibitor SMIFH2 prevents the formation of fertilization tubules. Fertilization tubule formation in *Chlamydomonas* occurs near the membrane at a site between the two flagella. Prior to fertilization tubule formation, this site is characterized by two parallel electron-dense regions called the membrane zone (immediately adjacent to the membrane) and doublet zone (slightly interior) (Goodenough and Weiss, 1975; Detmers *et al.*, 1983). In a mature fertilization tubule, the pointed ends of actin filaments are attached at the doublet zone (Detmers *et al.*, 1983) while the membrane zone is present at the far end of the extended fertilization tubule, near the F-actin barbed ends. As formins are typically membrane-anchored, CrFor1 is potentially localized to the membrane zone, which extends from the doublet zone following F-actin formation. Fertilization tubules are capable of partially forming in the presence of cytochalasin D (Detmers *et al.*, 1983), suggesting that actin polymerization is specifically important for extended formation and maturation of the fertilization tubule. CrFor1 could additionally be important for bundling the actin filaments in the fertilization tubule (Figure S1), creating a stable projection. Future work will involve determining the factors that regulate CrFor1 activity and other ABPs that are involved in proper organization of F-actin at that site.

ACKNOWLEDGEMENTS

We thank Susan Dutcher for helpful discussions, including confirmation that *Chlamydomonas* expresses CrFor1. This work was supported by National Institutes of Health grants R01 GM079265 (to D.R.K.), P20 GM104936 (to P.A.), NSF Graduate Student Fellowship DGE-1144082 (to J.R.C.) and Molecular and Cellular Biology Training Grant T32 GM007183 (to J.R.C. and C.T.S.).

METHODS

Plasmid construction

Constructs containing different components of the formin actin assembly domains (FH1 and FH2) were prepared for bacterial expression. The preparation of Cdc12(FH1FH2) and Cdc12(FH1) constructs has been described (Neidt *et al.*, 2009). The CrFor1 domain constructs were designed based on sequence analysis of the *Chlamydomonas* genome, and Expressed Sequence Tag analysis by Susan Dutcher (Washington University, St. Louis), and were optimized for bacterial expression and custom synthesized (DNA 2.0, Newark, California). All constructs were prepared by standard cloning procedures, consisting of PCR amplification (iProof, Bio-Rad Laboratories) from the commercially prepared DNA. Restriction enzyme cleavage sites and 6x His sequences were included in the reverse primers. PCR products were cloned using restriction enzymes into pET21a (EMD Biosciences) for expression. All amplified sequences were confirmed by sequencing.

Protein purification

All constructs of CrFor1 and CrPRF were expressed in BL21-Codon Plus (DE3)-RP (Agilent Technologies, Santa Clara, CA). Cdc12(FH1FH2) (Kovar and Pollard, 2004), SpPRF (Lu and Pollard, 2001), SpFus1 (Scott *et al.*, 2011), and CrPRF (Kovar *et al.*, 2001) were purified as described previously. CrFor1 constructs were His-tag affinity purified. CrFor1 constructs were expressed with 0.5 mM isopropyl ß-D-thiogalactopyranoside (IPTG; Sigma-Aldrich) for 16 hours at 16°C. Cells were resuspended in extraction buffer (50 mM NaH_2PO_4, pH 8.0, 500 mM NaCl, 10% glycerol, 10 mM imidazole, 10 mM betamercaptoethanol [ßME]) supplemented with 0.5 mM phenylmethylsulfonyl fluoride (PMSF) and protease inhibitors, sonicated, and homogenized in an Emulsiflex-C3 (Avestin, Ottawa, ON, Canada). The homogenate was spun and clarified at 30,000*g* for 15 minutes, then 50,000*g* for 30 minutes and incubated with Talon Metal Affinity Resin (Clontech, Mountain View, CA) for 1 hour at 4°C. The resin was loaded onto a disposable column and washed with 50 mL wash with extraction buffer. CrFor1 was then eluted with Talon elution buffer (50 mM NaH_2PO_4, pH 8.0, 500 mM NaCl, 10% glycerol, 250 mM imidazole, 10 mM ßME) and dialyzed into formin buffer (20 mM HEPES, pH 7.4, 1 mM EDTA, 200 mM KCl, 0.01% NaN3, and 1 mM DTT).

A_{280} of purified proteins was taken using a Nanodrop 2000c Spectrophotometer (Thermo-Scientific, Waltham, MA). Protein concentrations were determined based on extinction coefficients estimated from amino acid sequences using ProtParam (http://web.expasy.org/protparam/), or from previous studies: CrPRF: 19,190 M^{-1} (Kovar *et al.*, 2001), SpPRF: 20,065 M^{-1} (Lu and Pollard, 2001), CrFor1(FH1,FH2): 29,450 M^{-1}, CrFor1(3P,FH2): 24,200 M^{-1}, CrFor1(FH2): 24,400 M^{-1}, SNAP-CrFor1(3P,FH2): 44,920 M^{-1}, and Cdc12 (FH1,FH2): 51,255 M^{-1} (Kovar *et al.*, 2003). Protein concentrations of FH1 constructs Cdc12(FH1), CrFor1(FH1) , and CrFor1(3P) were determined by A_{205} in water ([(A_{205}FH1− A_{205}buffer)/30]/mol wt). Proteins were flash-frozen in liquid nitrogen and kept at -80°C. SNAP-CrFor1(3P,FH2) protein was labeled with SNAP-549 dye (New England Biolabs, Ipswich, MA) as per manufacturer's instructions prior to each TIRF experiment.

Actin was purified from rabbit or chicken skeletal muscle actin as previously described (Spudich and Watt, 1971). For pyrene assembly assays, actin was labeled with N-(1-Pyrene)Iodoacetamide (Life Technologies, Carlsbad, CA) on Cys-374. As the combination of CrFor1 in the presence of CrPRF selected against actin labeled on Cys-374, actin labeled with Alexa Fluor 488 on lysines (ThermoFisher Scientific, Waltham, MA) was used for TIRF microscopy experiments.

Pyrene assembly and disassembly assays

All pyrene assembly and disassembly assays were carried out in a 96-well plate, and the fluorescence of pyrene-actin (excitation at 364 nm and emission at 407 nm) was measured with a Spectramax Gemini XPS (Molecular Devices) or Safire2 (Tecan) fluorescent plate reader as described (Zimmermann *et al.*, 2016). For spontaneous assembly assays, a 15 µM mixture of 20% pyrene-labeled Mg-ATP-actin monomer with 100X anti-foam 204 (0.005%; Sigma) was placed in the upper well of a 96 well non-binding black plate. Formin and/or profilin, 10X KMEI (500 mM KCl, 10 mM $MgCl_2$, 10

mM ethylene glycol tetraacetic acid [EGTA], and 100 mM imidazole, pH 7.0), and Mg-Buffer G (2 mM Tris, pH 8.0, 0.2 mM ATP, 0.1 mM MgCl2 and 0.5 mM DTT) were placed in the lower row of the plate. Reactions were initiated by mixing contents of the lower wells the actin monomers in the upper wells with a twelve-channel pipetman (Eppendorf). For pyrene assembly assays involving SMIFH2, SMIFH2 was added to the lower wells containing CrFor1 prior to mixing the upper and lower wells.

For seeded assembly assays, 5.0 μM unlabeled Mg-ATP-actin was preassembled in the upper row of the plate, followed by addition of anti-foam, formin and/or profilin, and Mg-Buffer G. A 2.0 μM mixture of 20% pyrene-labeled actin with Mg-Buffer G was placed in the lower plate row. Mixing actin monomers in lower wells with pre-assembled actin filaments in upper wells initiated reactions.

For depolymerization assays, a 5.0 μM mixture of unlabeled and 50% pyrene-labeled Mg-ATP-actin monomers was preassembled in the upper row of the plate for two hours, followed by addition of anti-foam. Formin, 10X KMEI and Mg-Buffer G were placed in the lower plate row. Reactions were initiated by mixing lower wells with upper wells, diluting the pre-assembled filaments to 0.1 μM.

Profilin FH1 affinity assays

The affinity of profilin for formin(FH1) was determined by measuring the change in profilin's intrinsic tryptophan fluorescence by excitation at 295 nm and emission at 323 nm (Perelroizen *et al.*, 1994; Petrella *et al.*, 1996). Profilin (1.0 μM) was incubated with a range of poly-L-proline or formin(FH1) concentrations for 30 min, then profilin fluorescence was read in a Safire2 fluorescence plate reader and plotted versus formin(FH1) concentration. The fluorescence of formin(FH1) alone was subtracted from the fluorescence in the presence of profilin. Dissociation constants (K_d) were determined by fitting a quadratic function to the dependence of the concentration of bound profilin on the concentration of formin(FH1).

Polymerization and depolymerization rate determination

Actin assembly rates were determined from spontaneous assembly reactions by measuring the slopes of actin assembly following the lag phase to 50% of total actin assembly. Assembly rates from preassembled actin seeds were determined by a linear fit to the first 100 seconds of assembly. Depolymerization rates were determined by a linear fit to the first 100-300 seconds of the reaction.

The affinity of CrFor1 for barbed ends was determined as previously described (). We fit the plot of the dependence of the assembly or disassembly rate on formin concentration using the equation $V_i = V_{if} + (V_{ib} - V_{if})$ $((K_d + [\text{ends}] + [\text{formin}] - \sqrt{((K_d + [\text{ends}] + [\text{formin}])2 - 4[\text{ends}][\text{formin}])}/2[\text{ends}]))$, where V_i is the observed elongation or depolymerization rate, V_{if} is the elongation or depolymerization rate of free barbed ends, V_{ib} is the elongation or depolymerization rate of bound barbed ends, [ends] is the concentration of barbed ends, and [formin] is formin concentration. The nucleation efficiency was calculated by dividing the slope of the spontaneous assembly rate by $k+$ in the absence and presence of profilin and dividing by the formin concentration (Kovar *et al.*, 2006). Depolymerization rates are normalized to the rate of actin assembly alone and expressed as a percent of the standard actin assembly rate.

Fluorescence micrographs (rhodamine phalloidin)
Unlabeled Mg-ATP-actin was assembled as per standard spontaneous assembly reactions. Actin filaments were then incubated with 1 μM TRITC-Phalloidin (Fluka Biochemika, Switzerland) for 5 minutes. Reactions were terminated by diluting assembled filaments in fluorescence buffer (50 mM KCl, 1 mM $MgCl_2$, 100 mM DTT, 20 μg/ml catalase, 100 μg/ml glucose oxidase, 3 mg/ml glucose, 0.5% methylcellulose, and 10 mM imidazole, pH 7.0) and were absorbed to coverslips coated with 0.05 μg/μl poly-L-lysine. Fluorescence microscopy images were collected on an Olympus IX-81 microscope and cooled CCD camera (Orca-ER, Hamamatsu).

Low-speed sedimentation assays
Sedimentation assays were performed as previously described (Zimmermann *et al.*, 2016). 15 μM Mg-ATP actin monomers were spontaneously assembled for 1 hour in 10 mM imidazole, pH 7.0, 50 mM KCl, 5 mM $MgCl_2$, 1 mM EGTA, 0.5 mM DTT, 0.2 mM ATP and 90 μM $CaCl_2$ to generate F-actin. Filamentous actin was then incubated with CrFor1 or SpFus1 for 20 minutes at 25ºC and spun at 10,000g at 25ºC. Supernatant and pellets were separated by 15% SDS-PAGE gel electrophoresis and stained with Coomassie Blue for 30 minutes, destained for 16 hours and analyzed by densitometry with ImageJ.

TIRF microscopy
Time-lapse TIRF microscopy movies were obtained using a iXon EMCCD camera (Andor Technology, Belfast, UK) fitted to an Olympus IX-71 microscope with through-the-objective TIRF illumination as described (Zimmermann *et al.*, 2016). Mg-ATP-actin (20% Alexa 488-labeled) was mixed with a polymerization mix (10 mM imidazole (pH 7.0), 50 mM KCl, 1 mM MgCl2, 1 mM EGTA, 50 mM DTT, 0.2 mM ATP, 50 μM CaCl2, 15 mM glucose, 20 μg/mL catalase, 100 μg/mL glucose oxidase, and 0.5% (400 centipoise) methylcellulose) to induce F-actin assembly (Winkelman *et al.*, 2014). Where stated, formin or profilin was added to the polymerization mix prior to mixing with actin and initiating F-actin polymerization. The mixture was then added to a flow chamber and imaged at 10 s intervals at room temperature. For bead assays, Wsp1 and formin beads were prepared as previously described (Loisel *et al.*, 1999). Carboxylated Polybeads (Polysciences, Warrington, PA) were coated with Wsp1 or CrFor1 and flowed into the TIRF chamber prior to initiating the reaction.

Fertilization tubule assay
Wild type 137c (CC-125 mt+) *Chlamydomonas reinhardtii* cells were obtained from the Chlamydomonas Resource Center (University of Minnesota). To induce gametogenesis, cells were grown in M-N (M1 minimal media without nitrogen) overnight under growth lighting. Gametes were mixed with dibuteryl cAMP (13.5mM) and papaverine (135μM) to induce fertilization tubule formation along with different inhibitor preparations; untreated, 1% DMSO (solvent for all inhibitors), 10μM Latrunculin B, 10μM SMIFH2, 100μM SMIFH2, and 100μM CK-666. Cells were placed on a rotator under a LumiBar LED light source (LumiGrow, Inc) for 2hrs. After fertilization tubule induction, cells were adhered to coverslips coated with poly-lysine and fixed with 4% paraformaldehyde in 10mM HEPES. They were permeabilized with -20°C acetone, stained with 100nM Alexa Fluor 488 Phalloidin (Life Technologies) according to manufacturer protocols and

mounted on slides with Fluoromount-G (Southern Biotech) for imaging. Slides were imaged with a Nikon Ti-S widefield fluorescence microscope using a Plan Achromat 100x/1.25 NA oil immersion objective lens, a QICam fast 1394 CCD digital camera (QImaging) and NIS Elements software.

All cells in multiple fields of view (~50-100 cells per condition) were counted for presence of fertilization tubules using the ImageJ Cell Counter plugin to determine tubule percentage (#tubules/# total cells) x 100. Means and standard deviations are plotted for experiments done in triplicate. Results were analyzed with one way ANOVA and Dunnett's multiple comparison post hoc test. For fertilization tubule measurements, line segments were drawn onto projected FITC images and fit with splines using ImageJ. n>45 measurements were collected following a pixel to micron ratio conversion for the optical setup and compared using Kruskal-Wallis and Dunn's multiple comparison tests.

Figures

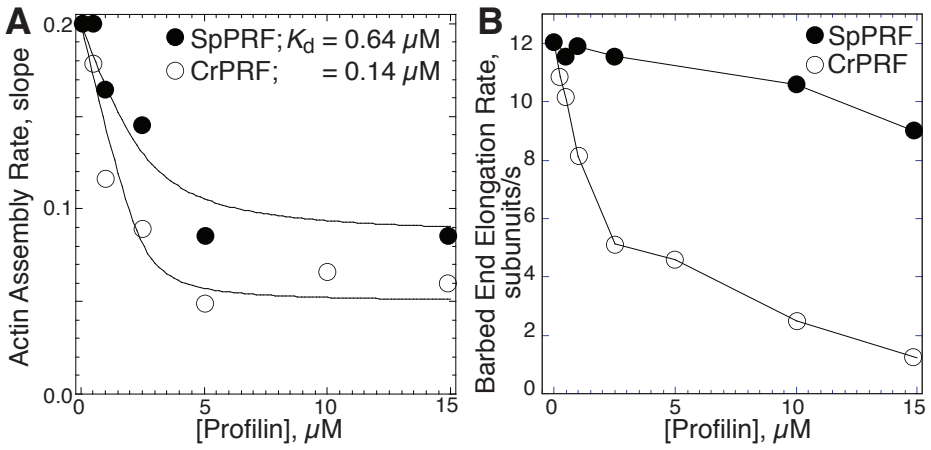

Figure 1: CrPRF inhibits nucleation and elongation of actin filaments.
(A) Slopes of spontaneous pyrene actin assembly assays (1.5 μM Mg-ATP actin, 20% pyrene labeled) with increasing concentrations of fission yeast profilin SpPRF or *Chlamydomonas reinhardtii* profilin CrPRF. Curve fits reveal affinities of SpPRF and CrPRF for actin monomer. (B) Barbed end elongation rates of 1.5 μM Mg-ATP actin (10% Alexa-488 labeled) in the presence of increasing concentrations of SpPRF or CrPRF, measured by TIRF microscopy.

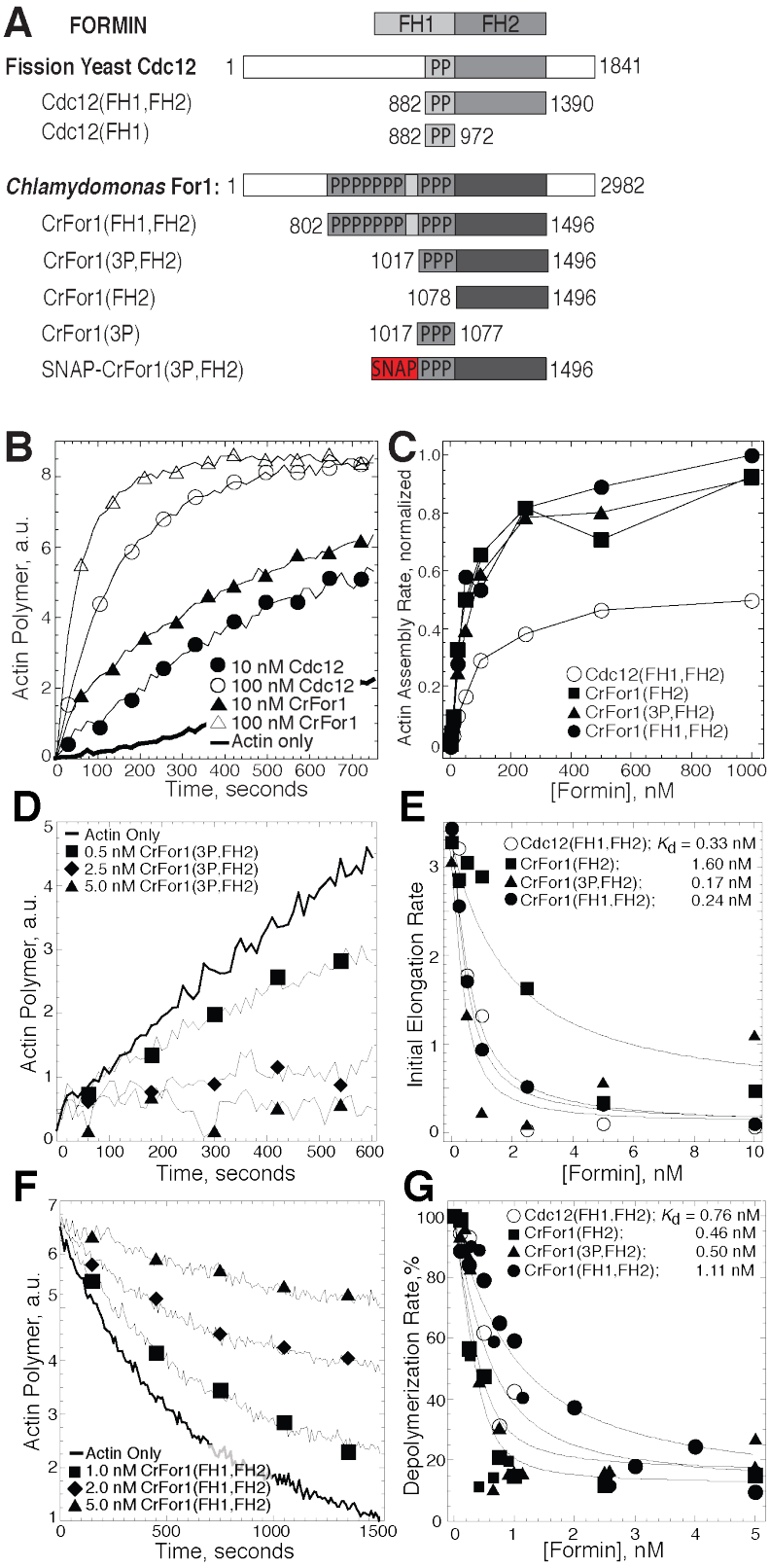
A
FORMIN
FH1
FH2
Fission Yeast Cdc12
1
PP
1841
Cdc12(FH1,FH2)
882
PP
1390
Cdc12(FH1)
882
PP
972
Chlamydomonas For1:
1
PPPPPPPP
PPP
2982
CrFor1(FH1,FH2)
802
PPPPPPPP
PPP
1496
CrFor1(3P,FH2)
1017
PPP
1496
CrFor1(FH2)
1078
1496
CrFor1(3P)
1017
PPP
1077
SNAP-CrFor1(3P,FH2)
SNAP
PPP
1496
B
Actin Polymer, a.u.
Time, seconds
10 nM Cdc12
100 nM Cdc12
10 nM CrFor1
100 nM CrFor1
Actin only
C
Actin Assembly Rate, normalized
[Formin], nM
Cdc12(FH1,FH2)
CrFor1(FH2)
CrFor1(3P,FH2)
CrFor1(FH1,FH2)
D
Actin Polymer, a.u.
Time, seconds
Actin Only
0.5 nM CrFor1(3P,FH2)
2.5 nM CrFor1(3P,FH2)
5.0 nM CrFor1(3P,FH2)
E
Initial Elongation Rate
[Formin], nM
Cdc12(FH1,FH2); Kd = 0.33 nM
CrFor1(FH2); 1.60 nM
CrFor1(3P,FH2); 0.17 nM
CrFor1(FH1,FH2); 0.24 nM
F
Actin Polymer, a.u.
Time, seconds
Actin Only
1.0 nM CrFor1(FH1,FH2)
2.0 nM CrFor1(FH1,FH2)
5.0 nM CrFor1(FH1,FH2)
G
Depolymerization Rate,%
[Formin], nM
Cdc12(FH1,FH2); Kd = 0.76 nM
CrFor1(FH2); 0.46 nM
CrFor1(3P,FH2); 0.50 nM
CrFor1(FH1,FH2); 1.11 nM

Figure 2: CrFor1 efficiently nucleates actin filaments that elongate slowly.
(A) Domain organizations and constructs used in this study of fission yeast formin Cdc12 and *Chlamydomonas reinhardtii* formin CrFor1. Numbers denote amino acid residues. Each "P" indicates a putative profilin binding site of at least 6 prolines within 8 residues. (B and C) Spontaneous assembly of 2.5 *μ*M Mg-ATP actin monomers (20% pyrene labeled). (B) Pyrene fluorescence over time for actin alone (thick curve), and with 10 (●) or 100 nM (○) Cdc12(FH1,FH2) or 10 (▲) and 100 nM (△) CrFor1(3P,FH2). (C) Dependence of the normalized actin assembly rate (slope) on the concentration of Cdc12(FH1,FH2) (○), CrFor1(FH2) (■), CrFor1(3P,FH2) (▲), and CrFor1(10P,FH2) (●). (D and E) Seeded assembly of 0.2 *μ*M Mg-ATP actin monomers (20% pyrene labeled) onto 0.5 μM preassembled filaments. (D) Pyrene fluorescence over time for actin alone (thick line) or in the presence of 0.5 (■), 1.0 (◆), or 2.5 nM (▲) CrFor1(3P,FH2). (E) Dependence of the initial barbed end assembly rate on formin concentration. Curve fits revealed equilibrium dissociation constants of 0.33 nM for Cdc12(FH1,FH2) (○), 1.6 nM for CrFor1(FH2) (■), 0.17 nM for CrFor1(3P,FH2) (▲), and 0.24 nM for CrFor1(10P,FH2) (●). (F and G) F-actin disassembly assays: depolymerization of 5 μM actin filaments (50% pyrene labeled) after dilution to 0.1 μM. (F) Depolymerization time-course in the absence (thick curve) or presence of 0.1 (■), 0.25 (◆), or 0.5 nM (▲) CrFor1(3P,FH2). (F) Dependence of the depolymerization rate on the concentration of the indicated formin. Curve fits revealed equilibrium dissociation constants of 0.76 nM for Cdc12(FH1,FH2) (○), 0.46 nM for CrFor1(FH2) (■), 0.50 nM CrFor1(3P,FH2) (▲), and 1.11 nM for CrFor1(10P,FH2) (●).

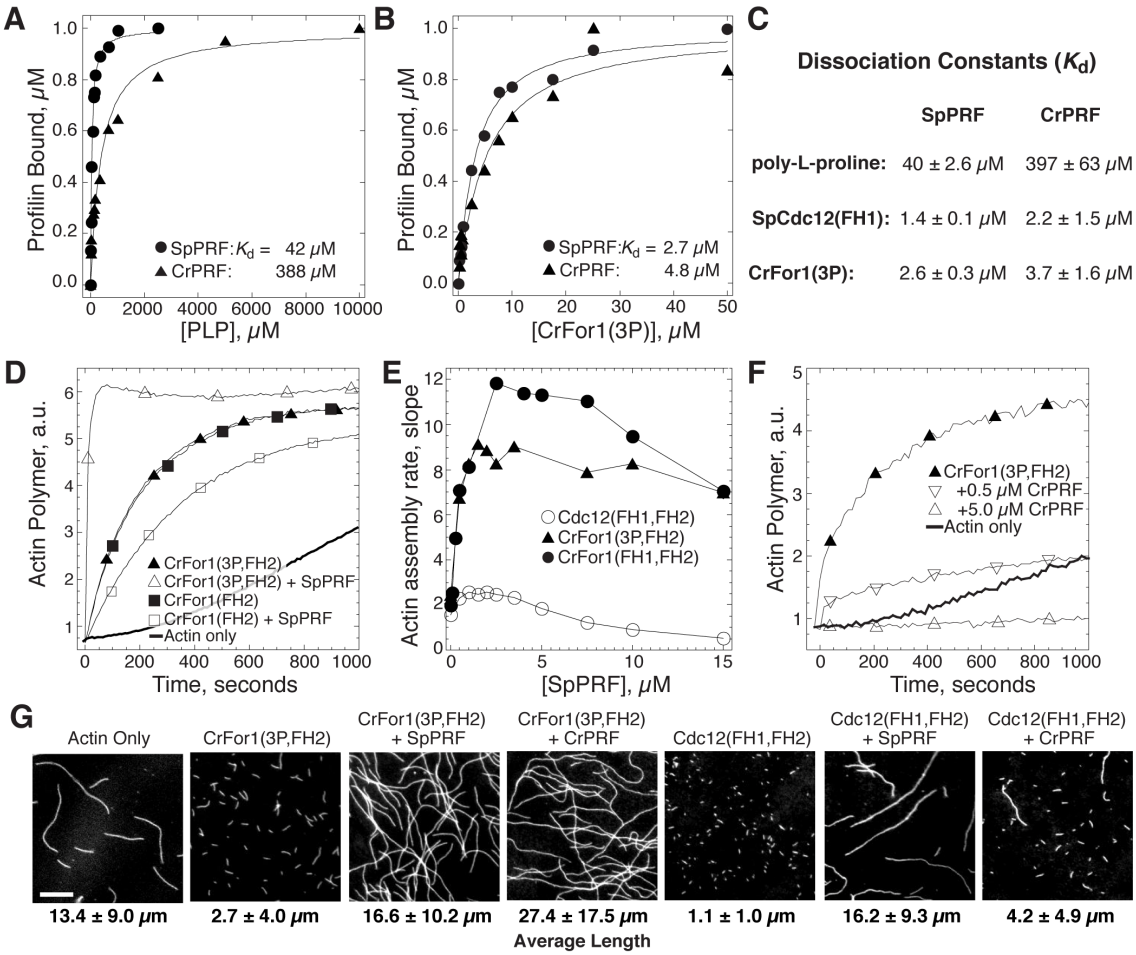

Figure 3: CrFor1 stimulates the assembly of profilin-actin. (A-C) Affinity of profilin for poly-L-proline and formin FH1 domains. Dependence of fission yeast SpPRF (●) and CrPRF (▲) intrinsic tryptophan fluorescence on the concentration of poly-L-proline (A) and CrFor1(3P) (B). (C) Average affinity of SpPRF and CrPRF for poly-L-proline, Cdc12(FH1) and CrFor1(3P); n≥3 experiments. (D-F) Spontaneous assembly of 2.5 μM Mg-ATP actin (20% pyrene-labeled). (D) Pyrene fluorescence over time for actin alone (thick curve), and with 10 nM CrFor1(FH2) in the absence (■) or presence (□) of 2.5 μM SpPRF, and with 10 nM CrFor1(3P,FH2) in the absence (▲) or presence (△) of 2.5 μM SpPRF. (E) Dependence of the actin assembly rate (slope) on the concentration of SpPRF for reactions containing 10 nM CrFor1(3P,FH2) (▲) or 10 nM Cdc12(FH1,FH2) (●). (F) Pyrene fluorescence over time for actin alone (thick curve), and with 10 nM CrFor1(3P,FH2) in the absence (▲), or presence of 0.5 μM (▽), or 5.0 μM (△) CrPRF. (G) Fluorescence micrographs of actin filaments taken 10 minutes after the initiation of the indicated reactions with 10 nM formin and 2.5 μM profilin. Samples were labeled with rhodamine-phalloidin and adsorbed to glass coverslips coated with poly-L-lysine. Scale bar, 5 μm.

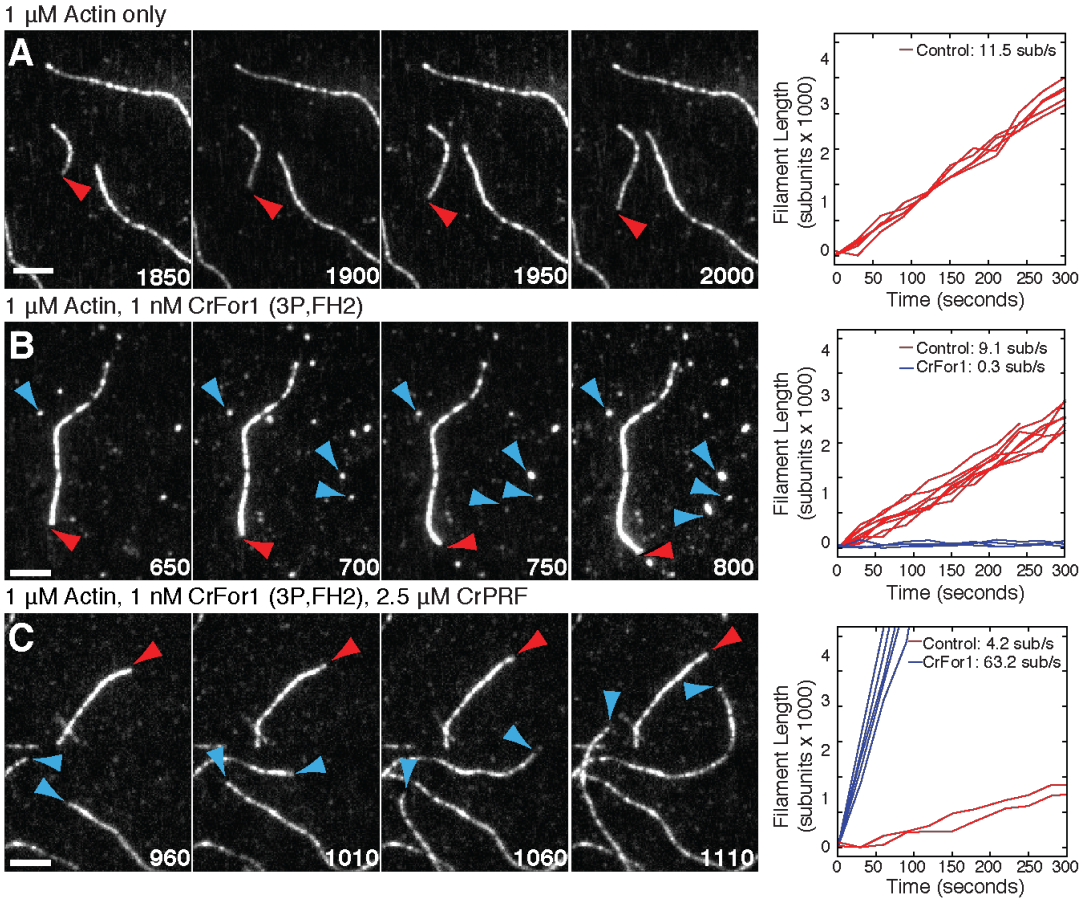

Figure 4: CrFor1 rapidly elongates actin filaments in the presence of CrPRF. **(A-C)** TIRF microscopy of 1 μM Mg-ATP actin (10% Alexa 488-labeled). (Left) Time lapse micrographs with time in seconds of actin alone **(A)**, with CrFor1(3P,FH2) **(B)**, and with CrFor1(3P, FH2) and CrPRF. Red and blue arrowheads denote control (formin independent) and CrFor1-dependent filaments, respectively. Scale bars, 5 μm. (Right) Rates of filament growth for control (red lines) and CrFor1-associated (blue lines) filaments.

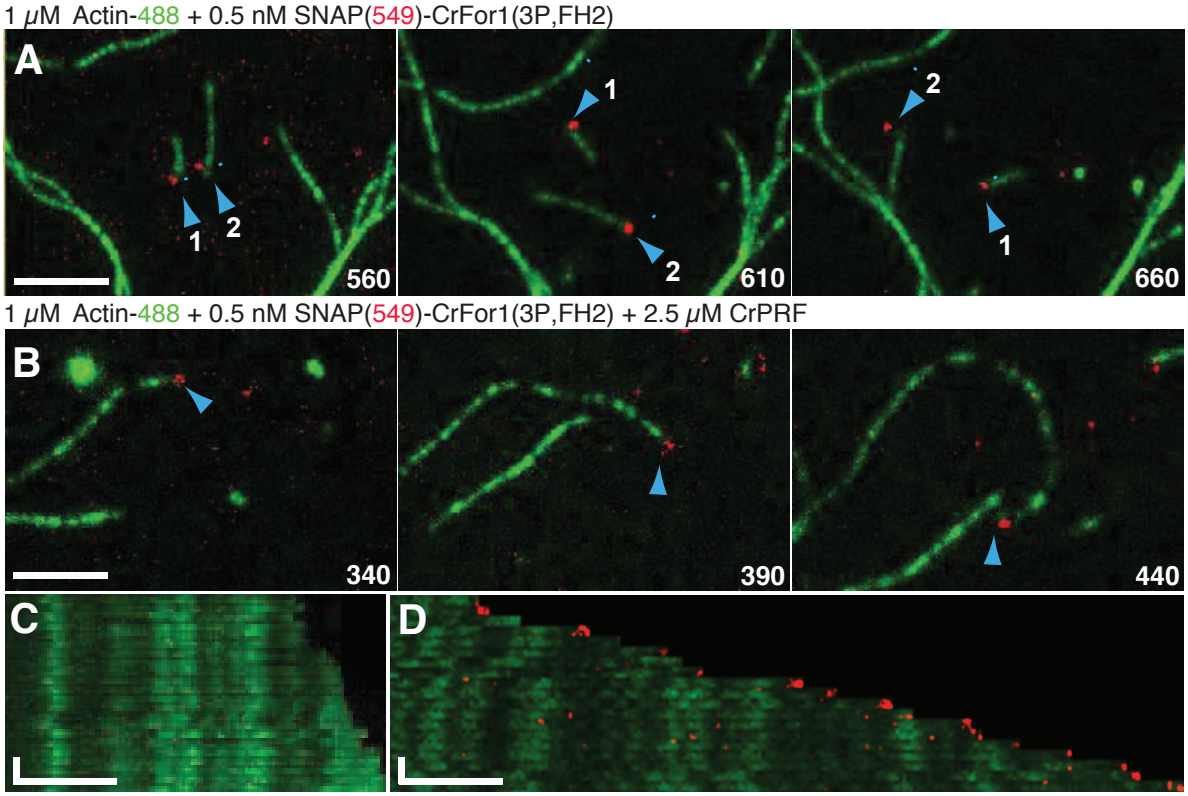

Figure 5: CrFor1 is processive in the absence and presence of CrPRF.
(A-D) Two-color TIRF microscopy of 1 μM Mg-ATP actin (10% Alexa 488-labeled) with 0.5 μM SNAP-CrFor1(3P,FH2) (549-labeled) in the presence or absence of 2.5 μM CrPRF. Blue arrowheads denote formin-bound filaments. **(A)** 0.5 μM SNAP-CrFor1(3P,FH2) alone. **(B)** 0.5 μM SNAP-CrFor1(3P,FH2) in the presence of 2.5 μM CrPRF. **(C and D)** Kymographs of control **(C)** and formin-bound **(D)** filaments from **(B)**. Scale bars, x-axis, 5 μm. Time bars, y-axis, 30 sec.

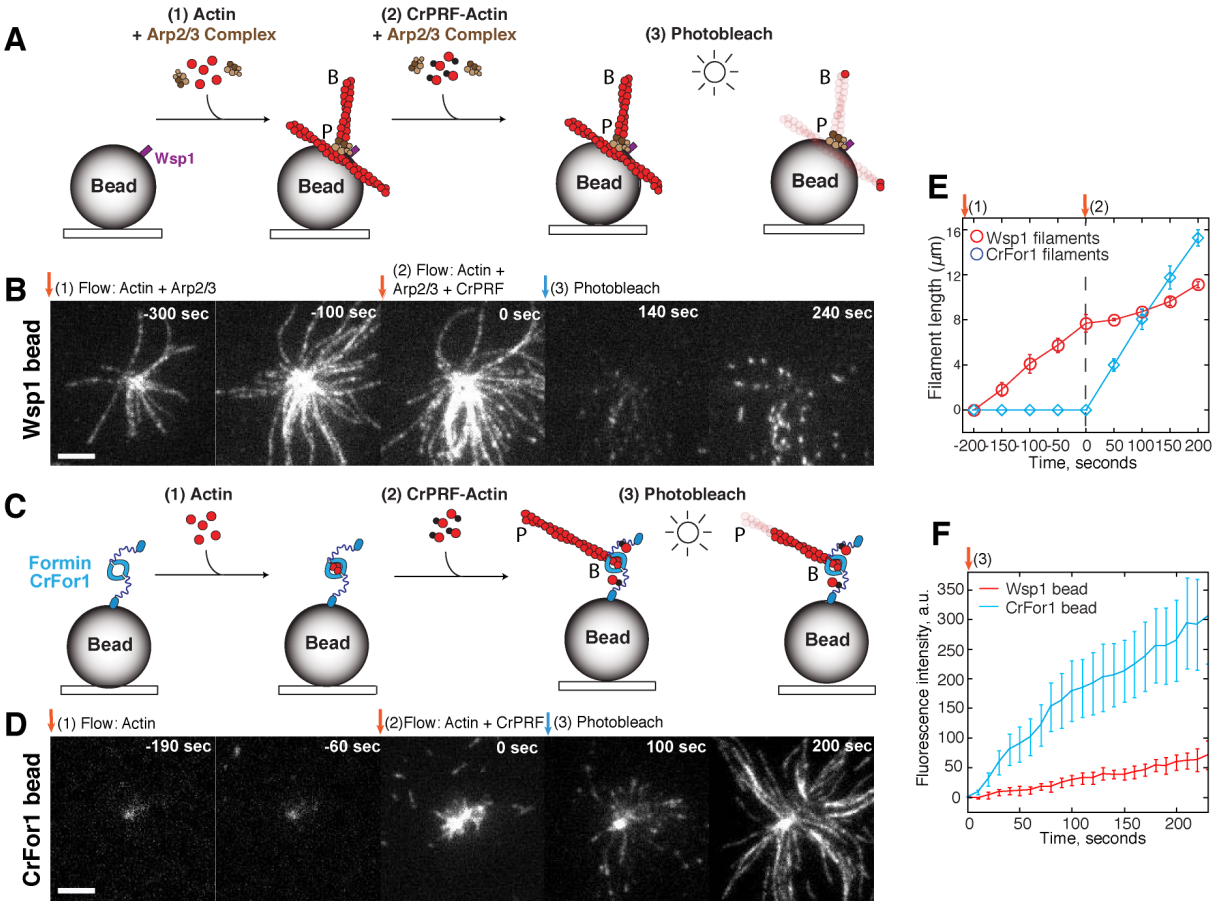

Figure 6: CrPRF facilitates formin- over Arp2/3 complex-mediated assembly. **(A-F)** TIRF microscopy bead assays. Fission yeast Arp2/3 complex activator Wsp1 or formin CrFor1 are adsorbed to a polystyrene bead and the effect of CrPRF-actin on network formation is observed. 'B' and 'P' indicate actin filament barbed and pointed ends, respectively. **(A-B)** Reactions containing beads coated with Wsp1. 1.5 μM Mg-ATP actin (10% Alexa 488-labeled) and 30 nM Arp2/3 complex is initially flowed into the chamber (1), followed by actin, Arp2/3 complex, and 2.5 μM CrPRF (2). Filaments are then photobleached to observe new assembly (3). **(C-D)** Reactions containing beads coated with CrFor1. Actin is initially flowed into the chamber (1), followed by actin and CrPRF (2), and then photobleached (3). **(E)** Actin filament length over time for filaments associated with Wsp1 (red) or CrFor1 (blue) beads. The initial flow of actin (1) and then actin with CrPRF (2) are indicated. Error bars=s.e., n=5 filaments. **(F)** Quantification of fluorescence intensity (actin assembly) at the surface of a Wsp1-coated (red) or CrFor1-coated (blue) beads following flow-in of CrPRF-actin and photobleaching. Error bars=??, n=? beads.

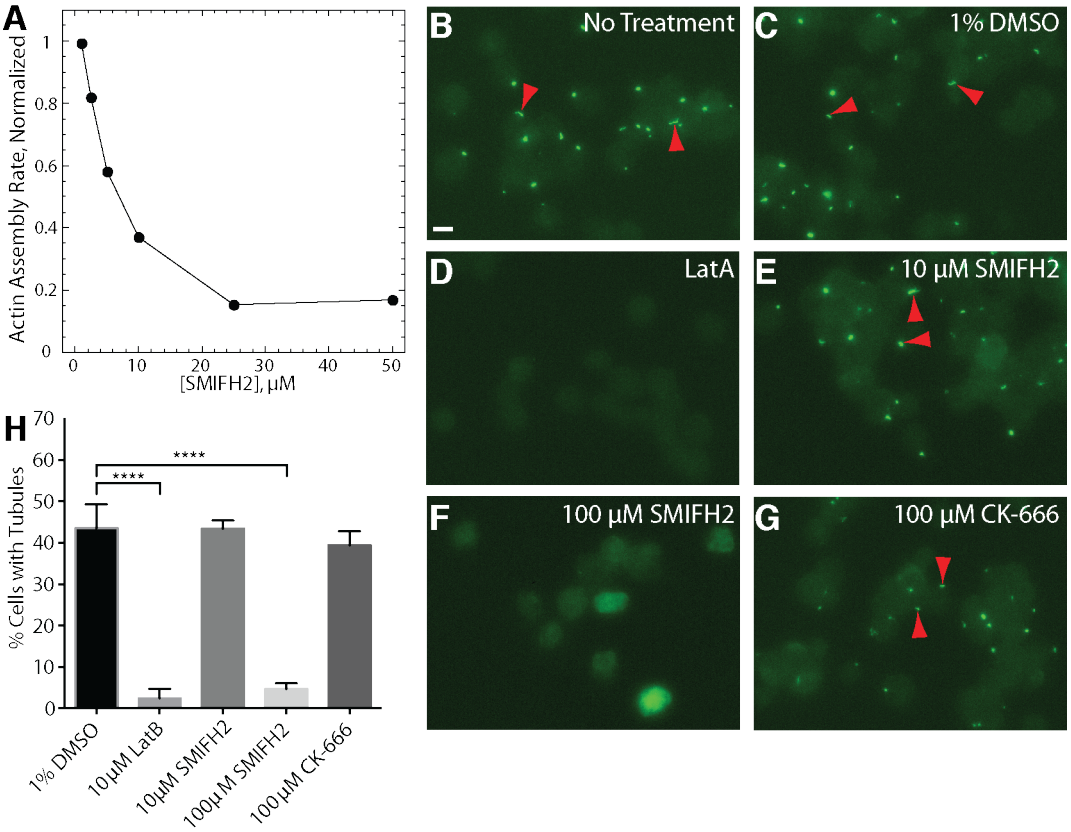

Figure 7: SMIFH2 formin inhibition disrupts fertilization tubules in *Chlamydomonas* gametes

(A) Normalized actin assembly rate of CrFor1(3P,FH2) (●) in the presence of increasing concentrations of formin inhibitor SMIFH2. **(B-F)** Representative fluorescent micrographs of *Chlamydomonas* gamete fertilization tubules (red arrowheads) labeled with the F-actin marker 488-phalloidin. Scale bar, 10 μm. **(B)** Untreated control. **(C)** 1% DMSO control. **(D)** 10 μM actin depolymerization drug Latrunculin B. **(E)** 10 μM formin inhibitor SMIFH2. **(F)** 100 μM SMIFH2. **(G)**100 μM Arp2/3 complex inhibitor CK-666. **(H)** Quantification of the percent of cells with fertilization tubules following indicated treatments. n=3 independent experiments. Error bars=S.D., ****p<0.0001.

References

Avasthi, P., Onishi, M., Karpiak, J., Yamamoto, R., Mackinder, L., Jonikas, M. C., Sale, W. S., Shoichet, B., Pringle, J. R., and Marshall, W. F. (2014). Actin Is Required for IFT Regulation in Chlamydomonas reinhardtii. Current Biology *24*, 2025–2032.

Bestul, A. J., Christensen, J. R., Grzegorzewska, A. P., Burke, T. A., Sees, J. A., Carroll, R. T., Sirotkin, V., Keenan, R. J., and Kovar, D. R. (2015). Fission yeast profilin is tailored to facilitate actin assembly by the cytokinesis formin Cdc12. Mol. Biol. Cell *26*, 283–293.

Breitsprecher, D., and Goode, B. L. (2013). Formins at a glance. J. Cell. Sci. *126*, 1–7.

Carlsson, L., Nystrom, L. E., Sundkvist, I., Markey, F., and Lindberg, U. (1977). Actin polymerizability is influenced by profilin, a low molecular weight protein in non-muscle cells. Journal of Molecular Biology *115*, 465–483.

Detmers, P. A., Carboni, J. M., and Condeelis, J. (1985). Localization of actin in Chlamydomonas using antiactin and NBD-phallacidin. Cell Motil. *5*, 415–430.

Detmers, P. A., Goodenough, U. W., and Condeelis, J. (1983). Elongation of the fertilization tubule in Chlamydomonas: new observations on the core microfilaments and the effect of transient intracellular signals on their structural integrity. The Journal of Cell Biology *97*, 522–532.

Goldschmidt-Clermont, P. J., Kim, J. W., Machesky, L. M., Rhee, S. G., and Pollard, T. D. (1991). Regulation of phospholipase C-gamma 1 by profilin and tyrosine phosphorylation. *251*, 1231–1233.

Goodenough, U. W., and Weiss, R. L. (1975). Gametic differentiation in Chlamydomonas reinhardtii. III. Cell wall lysis and microfilament-associated mating structure activation in wild-type and mutant strains. The Journal of Cell Biology *67*, 623–637.

Harper, J. D., McCurdy, D. W., Sanders, M. A., Salisbury, J. L., and John, P. C. (1992). Actin dynamics during the cell cycle in Chlamydomonas reinhardtii. Cell Motil. Cytoskeleton *22*, 117–126.

Kaiser, D. A., Vinson, V. K., Murphy, D. B., and Pollard, T. D. (1999). Profilin is predominantly associated with monomeric actin in Acanthamoeba. J. Cell. Sci. *112 (Pt 21)*, 3779–3790.

Kato-Minoura, T. E. A. (1998). Highly Divergent Actin Expressed in a Chlamydomonas Mutant Lacking the Conventional Actin Gene. 1–6.

Kato-Minoura, T., Hirono, M., and Kamiya, R. (1997). Chlamydomonas inner-arm dynein mutant, ida5, has a mutation in an actin-encoding gene. The Journal of Cell Biology *137*, 649–656.

Kollmar, M., Lbik, D., and Enge, S. (2012). Evolution of the eukaryotic ARP2/3 activators of the WASP family: WASP, WAVE, WASH, and WHAMM, and the proposed new family members WAWH and WAML. BMC Research Notes *5*, 88.

Kovar, D. R. (2006). Molecular details of formin-mediated actin assembly. Curr. Opin. Cell Biol. *18*, 11–17.

Kovar, D. R., and Pollard, T. D. (2004). Insertional assembly of actin filament barbed ends in association with formins produces piconewton forces. Proc Natl Acad Sci USA *101*, 14725–14730.

Kovar, D. R., Harris, E. S., Mahaffy, R., Higgs, H. N., and Pollard, T. D. (2006). Control of the assembly of ATP- and ADP-actin by formins and profilin. Cell *124*, 423–435.

Kovar, D. R., Kuhn, J. R., Tichy, A. L., and Pollard, T. D. (2003). The fission yeast cytokinesis formin Cdc12p is a barbed end actin filament capping protein gated by profilin. The Journal of Cell Biology *161*, 875–887.

Kovar, D. R., Yang, P., Sale, W. S., Drobak, B. K., and Staiger, C. J. (2001). Chlamydomonas reinhardtii produces a profilin with unusual biochemical properties. J. Cell. Sci. *114*, 4293–4305.

Lee, V. D., Finstad, S. L., and Huang, B. (1997). Cloning and characterization of a gene encoding an actin-related protein in Chlamydomonas. Gene *197*, 153–159.

Loisel, T. P., Boujemaa, R., Pantaloni, D., and Carlier, M. F. (1999). Reconstitution of actin-based motility of Listeria and Shigella using pure proteins. Nature *401*, 613–616.

Lu, J., and Pollard, T. D. (2001). Profilin binding to poly-L-proline and actin monomers along with ability to catalyze actin nucleotide exchange is required for viability of fission yeast. Molecular Biology of the Cell *12*, 1161–1175.

Mockrin, S. C., and Korn, E. D. (1980). Acanthamoeba profilin interacts with G-actin to increase the rate of exchange of actin-bound adenosine 5'-triphosphate. Biochemistry *19*, 5359–5362.

Mouneimne, G. *et al.* (2012). Differential remodeling of actin cytoskeleton architecture by profilin isoforms leads to distinct effects on cell migration and invasion. Cancer Cell *22*, 615–630.

Neidt, E. M., Scott, B. J., and Kovar, D. R. (2009). Formin Differentially Utilizes Profilin Isoforms to Rapidly Assemble Actin Filaments. J. Biol. Chem. *284*, 673–684.

Nolen, B. J., Tomasevic, N., Russell, A., Pierce, D. W., Jia, Z., McCormick, C. D., Hartman, J., Sakowicz, R., and Pollard, T. D. (2009). Characterization of two classes of small molecule inhibitors of Arp2/3 complex. Nature *460*, 1031–1035.

Onishi, M., Pringle, J. R., and Cross, F. R. (2016). Evidence That an Unconventional

Actin Can Provide Essential F-Actin Function and That a Surveillance System Monitors F-Actin Integrity in Chlamydomonas. Genetics *202*, 977-996.

Otomo, T., Tomchick, D. R., Otomo, C., Panchal, S. C., Machius, M., and Rosen, M. K. (2005). Structural basis of actin filament nucleation and processive capping by a formin homology 2 domain. Nature *433*, 488–494.

Perelroizen, I., Didry, D., Christensen, H., Chua, N. H., and Carlier, M. F. (1996). Role of nucleotide exchange and hydrolysis in the function of profilin in action assembly. J. Biol. Chem. *271*, 12302–12309.

Perelroizen, I., Marchand, J. B., Blanchoin, L., Didry, D., and Carlier, M. F. (1994). Interaction of profilin with G-actin and poly(L-proline). Biochemistry *33*, 8472–8478.

Petrella, E. C., Machesky, L. M., Kaiser, D. A., and Pollard, T. D. (1996). Structural requirements and thermodynamics of the interaction of proline peptides with profilin. Biochemistry *35*, 16535–16543.

Pollard, T. D., and Cooper, J. A. (1984). Quantitative analysis of the effect of Acanthamoeba profilin on actin filament nucleation and elongation. Biochemistry *23*, 6631–6641.

Rizvi, S. A., Neidt, E. M., Cui, J., Feiger, Z., Skau, C. T., Gardel, M. L., Kozmin, S. A., and Kovar, D. R. (2009). Identification and characterization of a small molecule inhibitor of formin-mediated actin assembly. Chem Biol *16*, 1158–1168.

Rotty, J. D., Wu, C., Haynes, E. M., Suarez, C., Winkelman, J. D., Johnson, H. E., Haugh, J. M., Kovar, D. R., and Bear, J. E. (2015). Profilin-1 Serves as a Gatekeeper for Actin Assembly by Arp2/3-Dependent and -Independent Pathways. Developmental Cell *32*, 54–67.

Scott, B. J., Neidt, E. M., and Kovar, D. R. (2011). The functionally distinct fission yeast formins have specific actin-assembly properties. Mol. Biol. Cell *22*, 3826–3839.

Spudich, J. A., and Watt, S. (1971). The regulation of rabbit skeletal muscle contraction. I. Biochemical studies of the interaction of the tropomyosin-troponin complex with actin and the proteolytic fragments of myosin. J. Biol. Chem. *246*, 4866–4871.

Suarez, C., and Kovar, D. R. (2016). Internetwork competition for monomers governs actin cytoskeleton organization. Nat Rev Mol Cell Biol, 1–12.

Suarez, C., Carroll, R. T., Burke, T. A., Christensen, J. R., Bestul, A. J., Sees, J. A., James, M. L., Sirotkin, V., and Kovar, D. R. (2015). Profilin Regulates F-Actin Network Homeostasis by Favoring Formin over Arp2/3 Complex. Developmental Cell *32*, 43–53.

Wilson, N. F., Foglesong, M. J., and Snell, W. J. (1997). The Chlamydomonas mating type plus fertilization tubule, a prototypic cell fusion organelle: isolation, characterization, and in vitro adhesion to mating type minus gametes. The Journal of

Cell Biology *137*, 1537–1553.

Winkelman, J. D., Bilancia, C. G., Peifer, M., and Kovar, D. R. (2014). Ena/VASP Enabled is a highly processive actin polymerase tailored to self-assemble parallel-bundled F-actin networks with Fascin. Proceedings of the National Academy of Sciences of the United States of America.

Zimmermann, D., Morganthaler, A. N., Kovar, D. R., and Suarez, C. (2016). In Vitro Biochemical Characterization of Cytokinesis Actin-Binding Proteins. Methods Mol. Biol. *1369*, 151–179.